JOURNAL OF Materials CHEMISTRY

The effect of temperature on the structural and textural evolution of sol–gel Al_2O_3–TiO_2 mixed oxides

J. Ascención Montoya,[a] Paz del Angel[a] and Tomás Viveros*[b]

[a]*Simulación Molecular, Instituto Mexicano del Petroleo, Eje Central 152, D.F. 07730, México*
[b]*Area de Ingeniería Química, UAM-Iztapalapa, Av. Michoacán y Purísima S/N Col., Vicentina, México, D.F. 09340, México. E-mail: tvig@xanum.uam.mx*

Received 10th October 2000, Accepted 14th November 2000
First published as an Advance Article on the web 7th February 2001

A series of Al_2O_3–TiO_2 mixed oxides with different TiO_2 concentrations (6%, 14% and 44% by weight) and the single oxides were prepared by the sol–gel method. The hydroxide precursors were transformed into their respective oxides and calcined at 500 °C, 700 °C and 900 °C. The evolution of the morphology, microstructure, texture and phase transformations were followed by X-ray diffraction, DTA–TGA, Scanning and Transmission Electron Microscopy with selected area electron diffraction and N_2 physisorption. The dried gels were formed by nanometric particles closely related to AlOOH (boehmite). The Ti^{4+} was highly dispersed and presumably incorporated into the AlOOH structure, affecting the morphology, the aggregation state and the atomic short range order. The mixed metallic oxides calcined at 500 °C were amorphous and formed by nanometric particles and pore sizes of about 2 nm. For these samples the surface area increased as the TiO_2 concentration increased especially at high Ti concentration. The sintering process started at 700 °C, resulting in particle and pore sizes growing from 2 nm to about 10 nm and the powders remained amorphous. At 900 °C both sintering and crystallization processes of TiO_2 and Al_2O_3 were accelerated by the Ti^{4+} segregation; rutile and α-alumina were present as separate phases. The textural properties were also affected, the surface area decreased and the average pore diameters increased for the same thermal treatment.

1. Introduction

The Al_2O_3–TiO_2 system is of interest for many applications, such as a catalyst support and as an advanced ceramic material. It was earlier reported to show high catalytic activity in the synthesis of aniline from phenol and ammonia and to possess increased acidity with respect to the single oxides.[1,2] The amount and the strength of the acid sites were found to be dependent on the TiO_2 concentration and the way TiO_2 was incorporated into the Al_2O_3 matrix.[2] On the other hand, reports show that TiO_2–Al_2O_3 oxides are promising alternative supports for HDS catalysts,[3–7] since these oxides improve the catalytic activity for sulfur removal and the resistance to abrasion in comparison with the traditional γ-Al_2O_3 support.[8] It has been reported that NiMo/TiO_2 catalysts exhibit higher hydrodesulfurization activity than NiMo/Al_2O_3 catalysts[9] with the additional advantage that the TiO_2-based catalysts present a high activity without presulfidation.[10] However, TiO_2 has a low thermal stability since the sintering process and anatase–rutile phase transition occur simultaneously at about 600 °C.

Since any catalytic application of the TiO_2–Al_2O_3-based catalyst is going to be strongly dependent on the surface area, porosity and relatively high thermal stability, various types of synthesis, such as impregnation of γ-Al_2O_3 or boehmite with $TiCl_4$ or $Ti(OBu^n)_4$, grafting (γ-Al_2O_3/$TiCl_4$),[3] coprecipitation of alkoxides[5,11] and sol–gel,[12,13] have been employed in order to achieve the best TiO_2 dispersion. TiO_2 interacts with Al_2O_3 to avoid TiO_2 segregation and crystallization. However, it is well known that TiO_2 is particularly effective in promoting both crystal growth and sintering of α-alumina.[14] Additionally, in the case of the single oxide alumina, the sintering and crystallization process depend on the morphology of the powder particles[15] and the reactivity can be promoted by the addition of different cations.[16] Recently, temperatures as low as 600 °C have been reported for the formation of α-alumina by doping γ-alumina with an alumina sol.[17]

A suitable liquid chemical method is necessary for preparing mixed oxides with enhanced properties resulting from the synergistic interaction between the individual oxides. The fundamental parameter is the magnitude of the interaction between the oxides, which will be directly related to the modification of textural, structural, acid–base and catalytic properties. The scale of interaction can range from the situation when the two oxides interact at the atomic level forming a solid solution, to the situation when large particles of the guest metal oxide are formed on the surface of the support. An intermediate case is when the formation of small particles or domains of the guest oxide grow inside the matrix of the support. The sol–gel method has proved to be a particularly powerful procedure to attain interactions at the atomic scale between different metal oxides.[13,18,19]

In this paper we report an investigation on the evolution of the textural and structural properties of mixed oxides of Al_2O_3 and TiO_2 prepared by the sol–gel method. The effects of Ti concentration and temperature on particle morphology, sintering, crystallization, crystal growth and thermal stability are presented and discussed.

2. Experimental

2.1. Synthesis

The Al_2O_3–TiO_2 system was prepared from the acid cohydrolysis of commercial aluminium tri-*sec*-butoxide $Al(OBu^s)_3$ (ATSB) and titanium(IV) tetrabutoxide $Ti(OBu^n)_4$ (TTB) (Aldrich), using isopropanol (Aldrich) as the solvent. In a 1 l glass reactor, aluminium and titanium alkoxides were dissolved in 300 ml of isopropanol at 25 °C. The mixture was maintained

 DOI: 10.1039/b008161m

under vigorous stirring for 2 hours, followed by the dropwise addition of a water, isopropanol and HNO_3 solution. The amounts of reactants used were in order to obtain the following molar ratios: $HNO_3/(ATSB+TTB)=0.2$; $H_2O/(ATSB+TTB)=20$; $ROH/(ATSB+TTB)=75$. After the gelling point, the transparent gels were aged without agitation for 24 hours, then they were dried with a room temperature air stream flowing through the reactor. Finally, the dried gels were carefully calcined in an air flow at 500 °C, 700 °C and 900 °C. Samples were named in terms of the titanium oxide concentration so that SA represents 100% alumina; SAT6 corresponds to 94 wt% Al_2O_3, 6 wt% TiO_2; SAT14 is 86 wt% Al_2O_3, 14 wt% TiO_2; SAT44 is 56 wt% Al_2O_3, 44 wt% TiO_2 and ST is 100% TiO_2. The temperature of calcination is also used to identify the samples, for example SA/500 is an alumina sample calcined at 500 °C.

2.2. Characterization

The DTA experiments were carried out on a Perkin Elmer DTA 1700 equipment, under an air flow, at a constant heating rate of 10 °C min^{-1}. The powder X-ray diffraction patterns were measured on a D-500 Siemens diffractometer with a graphite secondary beam monochromator, and the $CuK\alpha_2$ contribution was eliminated by DIFFRAC/AT software to obtain monochromatic $CuK\alpha_1$. Surface areas were measured by nitrogen adsorption at 75 K using Micromeritics Accusorb 2100 E equipment. Selected area diffraction patterns and bright field images coming from regions of about 2–20 μm were obtained in a JEOL 100 CX microscope. Scanning electron images were obtained in a JEOL JSM-35 CF microscope.

3. Results and discussion

3.1. Synthesis

The gels of the simple and mixed metallic hydroxides obtained were transparent and soft. The gelling times of the SA gel and ST gel were in the order of about 10 s and 6 min respectively. In the case of the mixed gels, the gelling time of the SA gel was not modified by the incorporation of $Ti(OBu^n)_4$ in the three compositions used. This fast gelation rate could be attributed to the fact that the alcohol interchange reaction presumably occurs when the $Al(OBu^s)_3$ and $Ti(OBu^n)_4$ alkoxides are dissolved in isopropanol, the OBu^s and OBu^n alkoxo groups are replaced by the OPr^i groups, in this way modifying the alkoxide structure which is more prone to nucleophilic attack, according to the reactions:[18,20]

$$Al(OBu^s)_3 + xPr^iOH \rightarrow Al(OBu^s)_{3-x}(Pr^iOH)_x + xBu^sOH$$

$$Ti(OBu^n) + yPr^iOH \rightarrow Ti(OBu^n)_{4-y}(Pr^iOH)_y + yBu^nOH$$

where x and y are in the ranges 0–3 and 0–4, respectively.

3.2. Thermal behaviour

TGA and DTA results are presented in Fig. 1 and 2, respectively. Below 500 °C, three different processes of weight loss were identified in the TGA experiments (Fig. 1). In the first one (≈25–200 °C), water and residual alcohol physically adsorbed on the solid surface are eliminated, and in this zone occurs the main weight loss of ≈70%. This process is strongly endothermic as shown in the DTA results (Fig. 2). The residual organic matter located in the structure of the hydroxide, on the surface and occluded in the micropores of the solids, is burned off in the range 200–500 °C representing about 30% of the total weight lost. Beyond 500 °C the samples lose practically no more weight. The behaviour of the DTA curves indicates that the dry gel was an aluminium oxyhydroxide, AlOOH, as has been previously reported.[21]

The DTA results show an exothermic peak that appears at

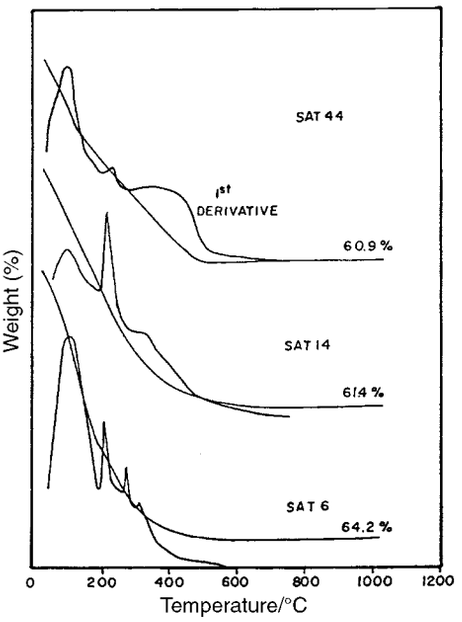

Fig. 1 Thermogravimetric analyses of dry sol–gel Al_2O_3–TiO_2 hydroxides.

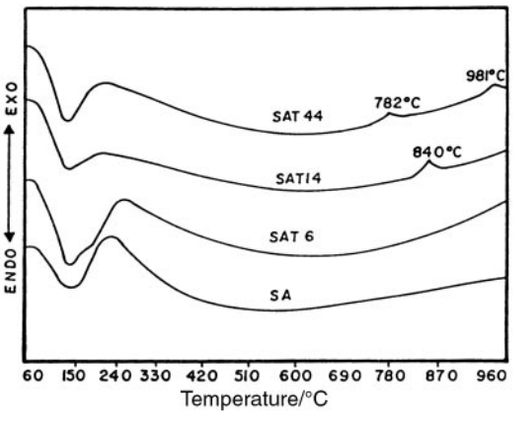

Fig. 2 Differential thermal analyses of dry sol–gel Al_2O_3–TiO_2 hydroxides.

840 °C in the SAT14 sample and two exothermic peaks at 782 °C and 981 °C detected in the case of the SAT44 sample (Fig. 2). No other peak was observed for the other samples (SA and SAT6) in the 500–800 °C range. The peak detected at the lower temperature could be assigned to the direct crystallization of amorphous TiO_2 into rutile and the higher temperature peak could be due to α-Al_2O_3 crystallization. These results suggest that during the thermal treatment TiO_2 is segregated from the Al_2O_3 particles forming nuclei of rutile and crystallizing before α-Al_2O_3. The first exothermic peak appears at a lower temperature as the TiO_2 concentration is increased. On the other hand, if the second peak in sample SAT44 corresponds to the formation of α-alumina, then it appears at a lower temperature than that reported for the single aluminium oxide.[22] Therefore, the formation of rutile TiO_2 induces the formation of α-Al_2O_3. The crystallization process then, is dependent on the temperature and the TiO_2 concentration.

It is also observed that the total weight loss increases as the TiO_2 concentration increases. According to this difference in total weight loss, the way in which the process was carried out and considering that all the samples were dried under the same conditions before the TGA experiments, it is expected that the porosity, the surface area and the aggregation state of the samples should be different.

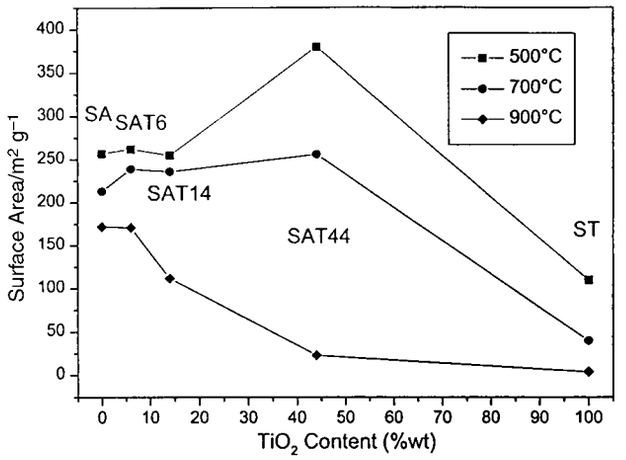

Fig. 3 Effect of temperature on the surface areas of single and mixed oxides.

3.3. Surface area and pore size distribution

The evolution of the surface area for the single and mixed oxides as a function of the calcination temperature and the TiO_2 concentration is represented in Fig. 3. The samples calcined at 500 °C show similar values of surface areas as pure alumina, up to a TiO_2 content of 14%, then it drastically increases from 250 $m^2\ g^{-1}$ to 380 $m^2\ g^{-1}$ for the SAT44 sample. After calcination at 700 °C there is a general decrease in surface area especially for the high Ti content sample. A further increase in the calcination temperature to 900 °C brings a more drastic decrease in the surface areas for all samples. As observed previously the sharpest surface area losses are found for the samples with high TiO_2 content and pure TiO_2.

The surface areas found in the mixed oxide samples are high and comparable to those reported by Miller and Lakshmi,[19] who used 2,4-pentanedione as a complexing/templating agent, and those recently reported by Escobar *et al.*[23] who used nitric acid as a hydrolysis catalyst. On the other hand, the areas are higher than those reported for samples prepared by precipitation of the alkoxides.[5,7,11]

Typical adsorption isotherms are shown in Fig. 4 and the corresponding pore size distributions (PSD) are given in Fig. 5 for the SAT44 sample. The adsorption isotherms are type IV, in the Brunauer classification.[24] It is observed that the low relative pressure point, where the adsorption and desorption branches coincide, is affected by the calcination temperature of the samples, appearing at higher relative pressures as the severity of the treatment increases, indicating the occurrence of capillary condensation at larger pores. This is confirmed by the pore size distributions shown in Fig. 5. This figure shows that the PSDs are unimodal and move toward larger pores with increasing calcination temperature of the sample. This effect is observed in all samples but is more pronounced as the TiO_2 concentration

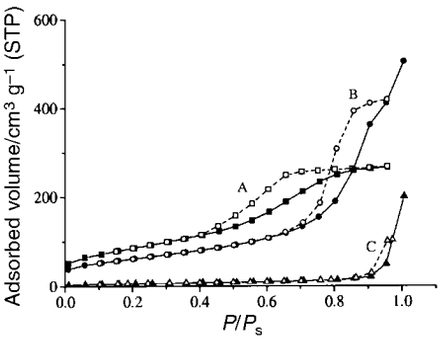

Fig. 4 N_2 adsorption isotherms of SAT44 sample calcined at 500 °C (A), 700 °C (B) and 900 °C (C).

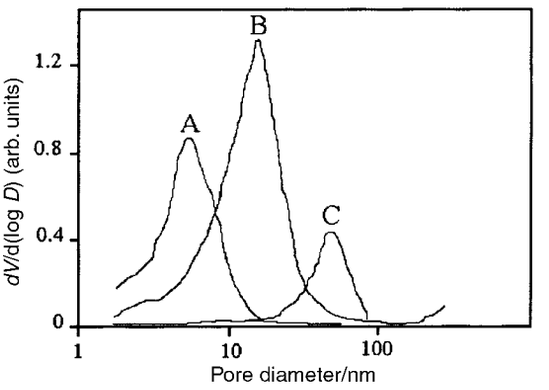

Fig. 5 Pore size distributions of SAT44 sample calcined at 500 °C (A), 700 °C (B) and 900 °C (C).

is increased. The average pore diameter was calculated to be 13.4 nm for alumina calcined at 500 °C (SA/500), 16.8 nm for SA/700 and 18.2 nm for SA/900, whereas for the high Ti content samples (SAT44) the equivalent pore diameters were 8 nm at 500 °C, 15.4 nm at 700 °C and 60 nm for the sample calcined at 900 °C.

3.4. Morphology, sintering and phase evolution

3.4.1. Morphology of dried gels. The grain morphology and the aggregation state of the dried gels were studied by SEM and TEM. These properties as well as the textural and structural characteristics of the solids are closely related to the synthesis parameters. SEM representative zones of the gels are given in Fig. 6 for SA and SAT6 samples. These micrographs show fibres and porous agglomerates of irregular size and shape, characteristic of the amorphous state of the gels. In the case of SA, the agglomerates are composed by irregular particles of $\approx$0.1–0.5 μm, but in the samples containing TiO_2 the particle

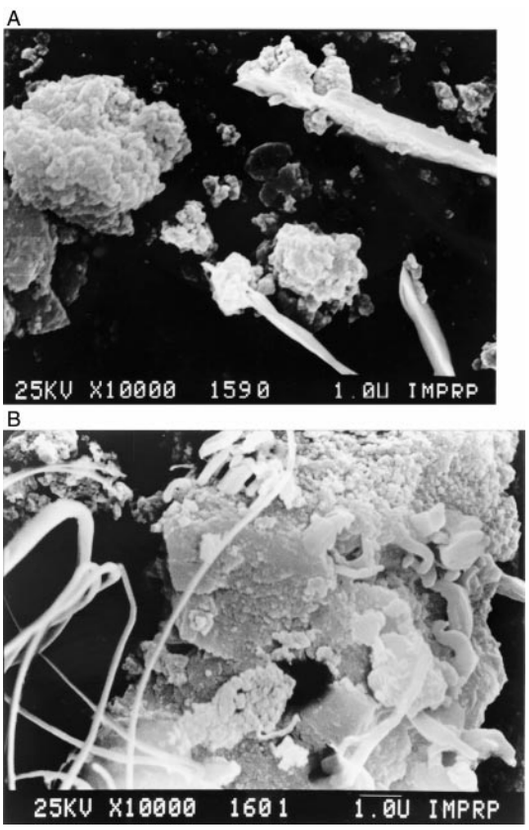

Fig. 6 SEM micrographs of dry non-calcined SA (A) and SAT6 (B) samples.

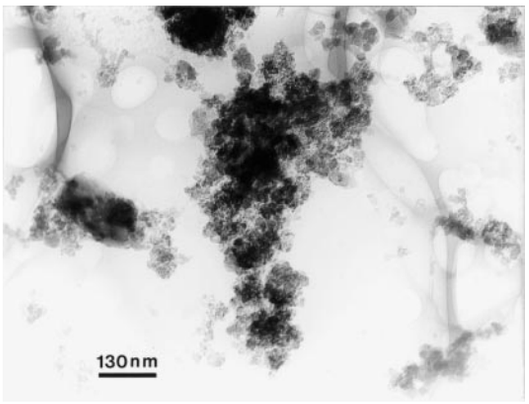

Fig. 7 TEM micrograph of dry non-calcined SA sample.

size decreases with the TiO_2 concentration. As a consequence the aggregation state is clearly affected in such a way that in the SAT44 sample the particle size is about 0.1 μm and forms a tabular material.

In order to observe the morphology of the elementary particles that compose the agglomerates, the samples were observed by TEM. The TEM of the SA sample is presented as a representative example (Fig. 7). It is observed that the agglomerates are formed by irregular elementary particles, with a grain size of *ca.* 2–4 nm, which are interconnected generating pores of irregular shape and average size *ca.* 3 nm. These nanometric particles did not generate diffraction patterns, suggesting they were in an amorphous state, although no attempt was made to obtain nano-diffraction spot analysis of individual particles. This kind of particle has a high surface/volume ratio. As a consequence, the surface free energy would be high and it is expected that their reactivity for sintering would also be high.[15]

3.4.2. Phase evolution followed by XRD. The effect of temperature on the structure of pure Al_2O_3, sample SA, followed by X-ray diffraction is shown in Fig. 8. It is observed that the SA sample remains amorphous up to 700 °C (Fig. 8A, B) but at 900 °C the amorphous material transforms into the γ-Al_2O_3 phase (10-425 JCPDS file) with a crystal size effect (Fig. 8C), as shown by the broad line widths of the sample pattern. The γ-Al_2O_3 crystal size was calculated from the (400) and (440) reflection widths, using the Scherrer equation,[25] to be about 4 nm and 6 nm respectively. This transformation sequence is different from that reported in the classical diagram of Al_2O_3 transformation, in which if a boehmite with large crystals is thermally treated between 475 °C and 600 °C, it is transformed into γ-Al_2O_3 having a crystal size similar to SA/900, but at a considerably lower temperature.[22] This result

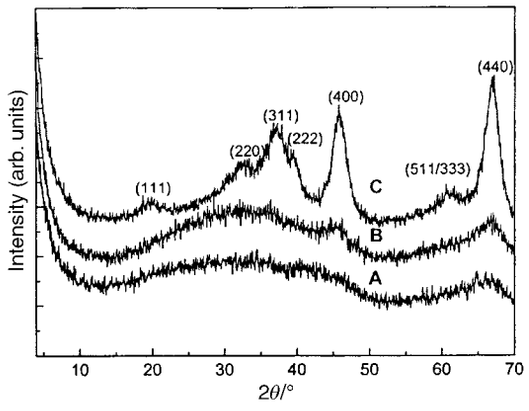

Fig. 8 X-Ray diffraction patterns of alumina (SA) calcined at 500 °C (A), 700 °C (B) and 900 °C (C).

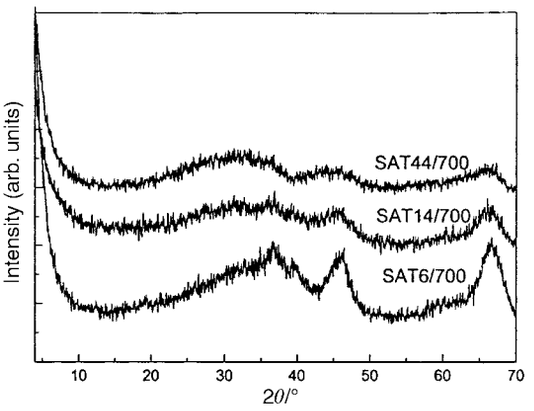

Fig. 9 X-Ray diffraction patterns of Al_2O_3–TiO_2 mixed oxides calcined at 700 °C.

indicates that the morphology and the particle size of the hydroxide precursor play important roles in both sintering and crystallization processes. A similar observation was made for γ-Al_2O_3 obtained from boehmites with different morphology,[15] thus γ-Al_2O_3 obtained from boehmite of small particles was more thermally stable than that coming from acicular pseudo-boehmite.

For alumina–titania samples calcined at 500 °C, XRD results show that all samples remain microcrystalline, with crystallite sizes below 3 nm. Although the diffractograms showed very broad line widths it could be observed that the crystal size decreased as the TiO_2 content increased. In fact, the SAT6/500 and SA/500 diffractograms were similar, suggesting the crystallite size was the same, and the effect of Ti^{4+} on the crystal size was not appreciable at this concentration. If sample SAT6 was calcined at 700 °C (SAT6/700 sample), the diffraction pattern (Fig. 9) matches the γ-Al_2O_3 phase (10-425 JCPDS file) with a crystal size of about 4.0 nm [obtained from the (440) reflection], which is clearly bigger than that of SA/700. This behaviour indicates that at this concentration TiO_2 favours the γ-Al_2O_3 crystallization and sintering processes. In contrast the SAT14/700 and SAT44/700 samples remain amorphous and TiO_2 is not detected at any TiO_2 concentration.

The diffraction patterns of the samples calcined at 900 °C are shown in Fig. 10. In sample SAT6/900 a mixture of pseudo δ and θ alumina phases was identified, the δ phase being the major component, and TiO_2 was not detected. For the sample SAT14/900 both pseudo δ and θ Al_2O_3 phases were also identified but now the major component was θ alumina. In this case TiO_2 was already detected in the rutile phase. The sample SAT44/900 crystallized to rutile and α-Al_2O_3 as segregated phases. Although both rutile and α-Al_2O_3 appear well crystal-

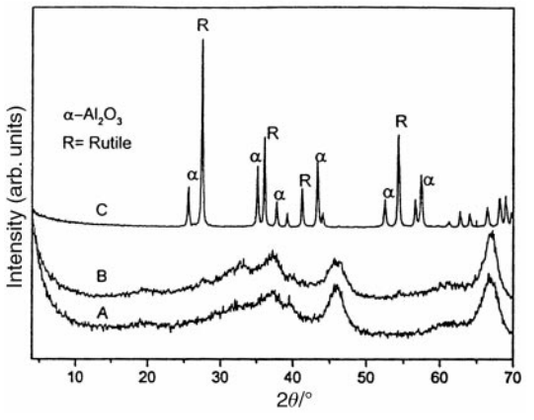

Fig. 10 X-Ray diffraction patterns of Al_2O_3–TiO_2 mixed oxides calcined at 900 °C [(A) SAT6/900, (B) SAT14/900, (C) SAT44/900].

lized, the low angle zone of the diffraction pattern, $2\theta = 4$–10°, is broad indicating that a fraction of the sample has small crystallites.

From these results it should be noted that: a) TiO_2 crystallized directly into rutile without passing through the anatase phase, and b) as a general trend, it can be established that Ti^{4+} incorporation into the alumina matrix promotes the amorphous–γ–δ–θ–α-Al_2O_3 crystallization process, which is a function of the TiO_2 concentration. Thus TiO_2 incorporation into alumina reduces the crystallization temperature of the α-Al_2O_3 in a process that depends on the TiO_2 concentration. Furthermore, it is possible to associate the direct rutile formation with a strong interaction between TiO_2 and Al_2O_3, otherwise TiO_2 would crystallize to the anatase phase at about 500 °C. In fact, this could be a criterion to establish the extent of TiO_2 integration into the alumina matrix.

3.4.3. Morphology and phase evolution followed by TEM. The aggregation state, shape and size of the nanoparticles in the single and mixed oxides were studied as a function of the thermal treatment by Transmission Electron Microscopy (TEM).

Fig. 11 shows a TEM micrograph of a representative zone of sample SA/500. This sample was composed mainly of nanometric particles of about 2 nm close to each other leaving free spaces or pores with diameters of about 2 nm. The porous aggregates formed suggest that the mechanism of condensation during the sol–gel synthesis was related to the monomer-cluster growth with a reaction-limited mechanism.[18] The aggregates were not faceted, and showed a very broad size distribution. They did not generate an electron diffraction pattern, which is characteristic of an amorphous material as has previously been shown by XRD. The 2 nm primary particles can be modelled assuming the Al^{3+} in tetrahedral or octahedral symmetry are spheres that form chains of four or five members.

The TEM results for the SAT6/500 mixed oxide showed that the individual particle size and the pore size were in the same range as those for SA/500, but the aggregates were bigger and looked like irregular flaky ridges. In contrast, in the SAT14/500 the aggregates were more compact and formed from individual particles of about 2–4 nm. In addition, there were some faceted aggregates, which are characteristic precursors of crystals. For the SAT44/500 sample, the particle and pore sizes were similar to those of SAT6/500 but the aggregates were thinner irregular flaky ridges. None of the mixed oxides produced XRD patterns, proving they were amorphous, and there were no crystalline zones, which would be difficult to detect by XRD. On the other hand, TiO_2 was not detected, which means that Ti^{4+} was still incorporated in the Al_2O_3 structure, otherwise at this temperature the TiO_2 would have crystallized into the anatase phase as was previously reported.[3] Furthermore, comparing the particle size, morphology and aggregation state of samples calcined at 500 °C to those observed for the pure SA hydroxide precursor, it can be said that during the dehydration process there was no sintering. The nanometric particles coarsened and formed chains of different lengths, leaving pores of irregular shape. Nortier *et al.*[26] suggested that the dehydroxylation process in large crystals of boehmite to form γ-alumina occurs by the reaction of two neighboring hydroxyls to form one molecule of water. This diffuses out of the crystal in the [100] direction, generating an OH vacancy and O^{2-} in excess. By a translation motion of the planes along the [001] direction the OH vacancy is occupied by other O^{2-} generating the fcc spinel lattice. They showed that during dehydration of boehmite crystals to γ-alumina, the particles retained their morphology.

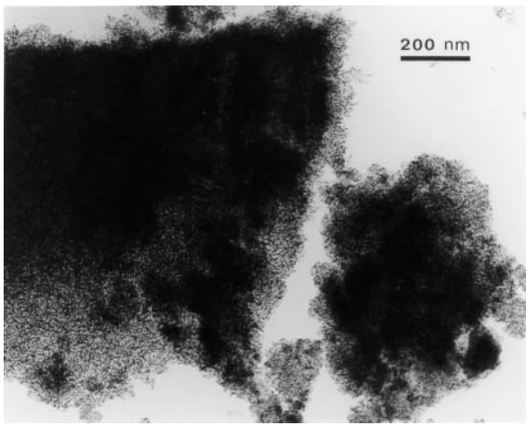

Fig. 11 TEM micrograph of alumina (SA) calcined at 500 °C.

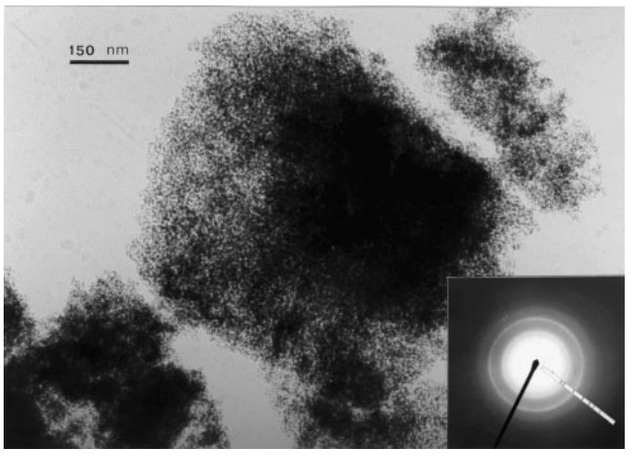

Fig. 12 TEM micrograph of alumina (SA) sample calcined at 900 °C.

The TEM results for samples calcined at 700 °C showed that the particle size had grown by grain boundary and necking to about 5–10 nm and the pore size had also increased to 5–10 nm. In this case the edges of the aggregates were more regular and in general they were denser, indicating that the sintering process had already started at this temperature. The selected area diffraction patterns of different zones showed that no crystalline material was formed.

The morphologies of the oxides calcined at 900 °C (SA/900, SAT6/900, SAT14/900 and SAT44/900) are shown in Fig. 12, 13, 14 and 15 respectively. Irregular aggregates of about 950 nm formed the SA/900 sample. The particle and pore sizes increased to 10–20 nm and 10 nm respectively. It is clear that both the individual particles and the aggregates had sintered. The diffraction patterns were rings, which are characteristic of

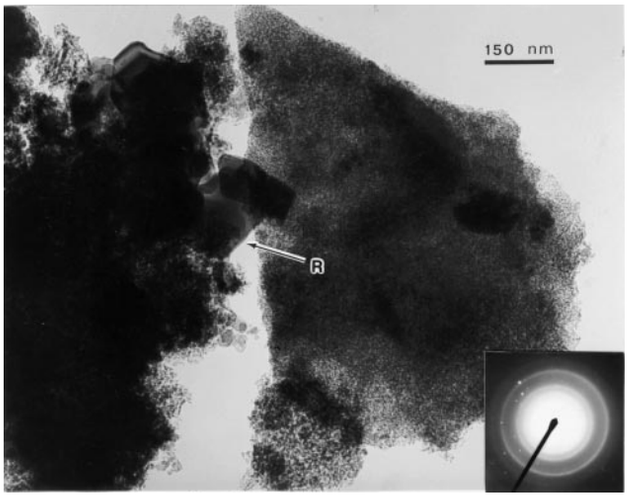

Fig. 13 TEM micrograph of alumina–titania (SAT6) sample calcined at 900 °C. Rutile (R) crystals are identified.

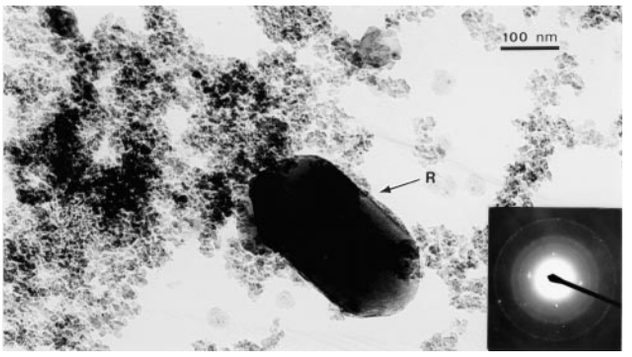

Fig. 14 TEM micrograph of alumina–titania (SAT14) sample calcined at 900 °C. A rutile crystal (R) and its diffraction pattern are shown.

polycrystalline material, identified as γ-Al_2O_3 (10-425 JCPDS file) without contamination of δ or θ phases. The crystallite size measured by XRD was about one half of the particle size.

In the SAT6/900 sample (Fig. 13) two phases were found. Agglomerates of about 1 μm size formed one phase with regular edges indicating that the formation of crystals had started. The particle size had grown to about 8 nm and the pore size to about 10 nm. Details of the morphology showed there were areas where the particles had sintered eliminating the porosity. It was also observed that the particles were forming rings, leaving open pores mainly of 6–7 nm in size, probably as a result of the coarsening process, so that an important pore fraction might be inaccessible to large molecules such as N_2, NH_3, *etc.* This morphology was similar to that of SA/900. On the other hand crystals of about 55 nm, which contrasted with the alumina morphology, formed the second phase. The diffraction patterns obtained were mainly rings but in some cases symmetric spots also appeared. The rings were identified as a mixture of δ and θ phases of Al_2O_3, and the patterns of the spots corresponded to rutile TiO_2 in the form of perfect faceted hexagonal crystals. The XRD technique could not detect the rutile phase, since the amount of TiO_2 rutile crystals was low and the alumina phases produce an intense background. In the case of the sample SAT14/900, the presence of rutile crystals was more evident and the crystals were of about 170 nm by 300 nm as can be observed in Fig. 14. The diffraction patterns again showed both rings belonging to polycrystalline δ and θ phases of Al_2O_3 and symmetrical spots corresponding to the rutile phase. The morphology of the alumina fraction was closely related to that of SAT6/900 but the average particle size was about 10 nm and there were more dense zones.

In the sample with the highest TiO_2 content, SAT44/900, for which XRD showed the presence of rutile and corundum phases, TEM micrographs (Fig. 15) showed that both phases were growing by a secondary recrystallization process and two different morphologies were observed. The first, presented in Fig. 15A, is composed by the coarser, very large and well faceted crystals (>50 nm) leaving pores bigger than 80 nm. Both crystal size and pore size distributions were very broad. The second morphology (Fig. 15B) was of the type observed in its low temperature precursors leaving a considerable fraction of pores. In both morphologies the selected area diffraction patterns were identified as a mixture of rutile and corundum, and since they have similar densities (corundum $= 3.96$ g cm^{-3}, rutile $= 4.25$ g cm^{-3}) it is not possible to distinguish between the individual crystals of the two phases. The diffraction pattern obtained from the material shown in Fig. 15A is typical of a polycrystalline material with well defined and randomly oriented large crystals (of about 50 nm or larger). The larger and equiaxial crystals (Fig. 15A) grow by consuming the material of the matrix of smaller crystals, shown in Fig. 15B.

An interesting aspect is that Ti^{4+} does not modify the topotactic transformation, and the coarsening of the microparticles observed in the transformation of the amorphous aluminium hydroxide as well as in the pseudo-boehmite to γ–δ–θ-Al_2O_3 transition phases is in agreement with the findings of Brinker and Scherer.[18]

On the other hand, considering that in all the samples the particle and the pore sizes are similar (2 nm), the increase in the surface area can be attributed to the effect of Ti^{4+} which hinders the formation of the typically inaccessible porosity observed in amorphous alumina.[18]

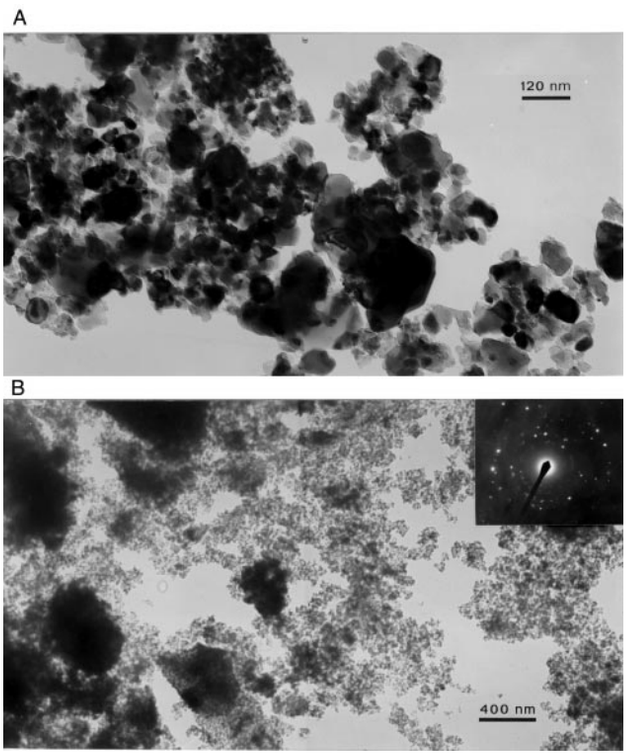

Fig. 15 TEM micrographs of (A) alumina–titania (SAT44) sample calcined at 900 °C, and (B) rutile and α-alumina microcrystals and their diffraction pattern (inset).

4. Conclusions

The effects caused by the sol–gel incorporation of Ti^{4+} into Al_2O_3 on the sintering process, crystal growth and thermal stability have been studied. The particle size of the amorphous aluminium hydroxide was not affected by the presence of Ti^{4+}, but the short range atomic order in the particles, which was boehmite-like, and the particle aggregation state were clearly modified.

The mixed metal oxides calcined at 500 °C remained microcrystalline The sintering of the nanometric particles started at 700 °C, the pore size increased and the surface area decreased, the biggest decrease being for the highest Ti^{4+} content. Beyond this temperature, TiO_2 formed nuclei and crystallized directly to the rutile phase without going through anatase. The crystallization temperature of rutile decreased as the TiO_2 concentration increased. The crystallization of rutile accelerated the sintering of alumina and the crystallization of α-Al_2O_3.

The sol–gel process, under the current synthesis parameters, is an effective method of obtaining a nanometric particle size powder with a narrow size distribution, and it is particularly valuable for the preparation of well dispersed Ti^{4+} in alumina with an open porosity and high surface area. However, the solid solution is thermally unstable beyond 700 °C and TiO_2 acts as a promoter of sintering and α-Al_2O_3 crystal growth.

Acknowledgements

We thank the financial support of Conacyt through the project 400200-5-4472, and IMP through the FIES program (project 98-31-III). T. V. wishes to thank Conacyt and UAM-I for support during sabbatical leave.

References

1 K. Shibata, T. Kiyoura, J. Kitagawa, T. Sumiyoshi and K. Tanabe, *Bull. Chem. Soc. Jpn.*, 1973, **46**, 2985.
2 E. Rodenas, T. Yamaguchi, H. Hattori and K. Tanabe, *J. Catal.*, 1981, **69**, 434.
3 W. Zhaobin, X. Qin, G. Xiexian, E. L. Sham, P. Grange and B. Delmon, *Appl. Catal.*, 1990, **63**, 305.
4 W. Zhaobin, X. Qin, G. Xiexian, P. Grange and B. Delmon, *Appl. Catal.*, 1991, **75**, 179.
5 J. Ramirez, L. Ruiz-Ramirez, L. Cedeño, V. Harle, M. Vrinat and M. Breysse, *Appl. Catal.*, 1993, **93**, 163.
6 R. J. Rigge, J. R. Graham and Y. J. Steve, *Eur. Pat. Appl.*, 0 339 640 A1, 1989.
7 J. Ramirez and A. Gutierrez-Alejandre, *J. Catal.*, 1997, **170**, 108.
8 R. W. Geoffry, W. Village and M. Kayamoto, *US Pat.*, 4 196 101, 1980.
9 K. Y. S. Ng and E. Gulari, *J. Catal.*, 1985, **95**, 33.
10 S. Masuda and A. Kato, *Appl. Catal.*, 1983, **8**, 149.
11 A. Gutierrez-Alejandre, M. Gonzalez-Cruz, M. Trombetta, G. Busca and J. Ramirez, *Microporous Mesoporous Mater.*, 1998, **23**, 265.
12 T. Woignier, P. Lespade, J. Phalippou and R. Rogier, *J. Non-Cryst. Solids*, 1988, **100**, 325.
13 J. A. Montoya, J. M. Domínguez, J. Navarrete, I. Schifter, T. Viveros, D. Chadwick and K. Zeng, *J. Sol–Gel Sci. Technol.*, 1994, **2**, 431.
14 R. D. Bagley, I. E. Cutler and D. L. Johnson, *J. Am. Ceram. Soc.*, 1970, **53**, 136.
15 I. I. M. Tijburg, H. De Bruin, P. A. Elberse and J. W. Geus, *J. Mater. Sci.*, 1991, **26**, 5945.
16 O. A. Kirichenko, V. A. Usahakov and E. M. Moroz, *Kinet. Catal.*, 1993, **34**, 663.
17 H. J. Youn, J. W. Jang, I. T. Kim and K. S. Hong, *J. Colloid Interface Sci.*, 1999, **211**, 110.
18 C. J. Brinker and G. W. Scherer, *Sol–Gel Science, the physics and chemistry of sol–gel processing*, Academic Press, New York, 1990.
19 J. M. Miller and L. J. Lakshmi, *J. Phys. Chem. B*, 1998, **102**, 6465.
20 D. C. Bradley, R. C. Methrotra and D. P. Gaur, *Metal Alkoxides*, Academic Press, New York, 1978.
21 O. Rodriguez, F. Gonzalez, P. Bosch, M. Portilla and T. Viveros, *Catal. Today*, 1992, **14**, 243.
22 B. C. Lippens and J. J. Steggerda, in *Physical and Chemical Aspects of Adsorbents and Catalysts*, Academic Press, New York, 1970.
23 J. Escobar, J. A. De los Reyes and T. Viveros, *Ind. Eng. Chem. Res.*, 2000, **39**, 666.
24 J. A. Moulijn, P. W. N. M. van Leeuwen and R. A. van Santen, *Catalysis, An Integrated Approach to Homogeneous, Heterogeneous and Industrial Catalysis*, Elsevier, Amsterdam, 1993.
25 H. P. Klug and L. E. Alexander, *X-ray Diffraction Procedures*, J. Wiley, New York, 1954.
26 P. Nortier, P. Fourre, A. B. M. Saad, O. Saur and J. C. Lavalley, *Appl. Catal.*, 1990, **61**, 141.